J Mater Sci (2010) 45:2449–2455
DOI 10.1007/s10853-010-4216-y

Mechanical, electrical, thermal performances and structure characteristics of flexible graphite sheets

Xing Hai Wei · Lang Liu · Jin Xi Zhang · Jing Li Shi · Quan Gui Guo

Received: 30 July 2009 / Accepted: 8 January 2010 / Published online: 21 January 2010

Abstract The mechanical, electrical, and thermal performances of flexible graphite sheets (FGS) derived from $HClO_4$-graphite intercalation compounds were characterized by measuring their tensile strength, electrical resistivity, and thermal conductivity. Results show that these performances are closely related to the density of sheets and exfoliated volume (EV) of exfoliated graphite. Enhancing density of sheets tends to improve their in-plane tensile strength, electrical, or thermal performance while using the exfoliated graphite of low EV to prepare sheets is prone to resulting in low in-plane tensile strength but high electrical or thermal performance. The structure characteristics of FGS were characterized by using X-ray diffraction, Raman spectroscopy, and scanning electron microscopy. The X-ray diffraction results show that the average interlayer spacing of graphite microcrystals for sheets, d_{002}, is 3.357 Å which is the same as that of natural graphite flake, but the stacking height of sheets, Lc, is lower than that of natural graphite. The Raman spectra indicate that sheets has both disorder peak and graphite one and the intensity ratio of them is ca. 0.06, which is almost the same as that of natural graphite, but higher than that of exfoliated graphite.

X. H. Wei (✉) · L. Liu · J. X. Zhang · J. L. Shi · Q. G. Guo
Key Laboratory of Carbon Materials, Institute of Coal Chemistry, Chinese Academy of Sciences, 030001 Taiyuan, China
e-mail: weixinghai@sxicc.ac.cn

X. H. Wei
Graduate School of Chinese Academy of Science, 100039 Beijing, China

Introduction

Flexible graphite sheets (FGS) provided characteristic advantages, such as flexibility, compactibility, resilience, and easily forming into various shapes, in addition to the original properties of graphite, i.e., lubricity, chemical and thermal stability, electrical and thermal conductivity, etc. [1]. FGS, used industrially, is based on H_2SO_4-graphite intercalation compound (GIC). Its main utilization is in sealing materials, where it presents many advantages over asbestos [2–4]. Therefore, it may be a good replacement of asbestos gaskets, particularly in the places where fire safety is demanded. It is also superior to conventional elastomeric bonded gaskets, because it is more thermally stable and chemically inert with considerably less creep relaxation. Due to the flexibility, resiliency, FGS tends to have a good compatibility with its mating material. Due to its microstructure involving graphite layers that are preferentially parallel to the surface of the sheet, FGS has high electrical and thermal conductivities in the plane of the sheet. Because graphite layers are some what connected perpendicular to the sheet (i.e., the honeycomb microstructure of exfoliated graphite), FGS is electrically and thermally conductive in the direction perpendicular to the sheet (although not as conductive as the plane of sheets) [5]. The flexibility, resiliency, and compatibility along with high thermal and electrical conductive potentialities make it possible for FGS to be utilized in the electric industry as heat sink or thermal interface materials. In view of the above mentioned these features of FGS, especially its in-plane thermal conductive property, together with mechanical and electrical properties which are required as a material were discussed to give a good understanding for this kind of flexible material. In carbon material family, FGS is the only two-dimension oriented flexible material

that can be produced in a large scale compared to other carbon materials. The producing method and the characteristics of exfoliated graphite are probably responsible for the flexible property of FGS. First, there are no adhesives involved in the shaping process of FGS. Second, exfoliated graphite particles have considerable porosity [6–12]. The preparation of FGS includes: the synthesis of GICs), thermally treatment of GIC to form exfoliated graphite, and the compressing exfoliated graphite to form FGS. Here, a method, different from one used industrially, was adopted. The reason why $HClO_4$ rather than H_2SO_4-GIC was used is in that: (1) the perchloric acid intercalant is more readily vaporized than sulfuric acid upon heating due to lower boiling point, thus the exfoliated graphite, and then the resultant FGS having higher purity, as is very important to make FGS with high electrical and thermal conductivities. (2) The intercalating reaction of $HClO_4$ with natural graphite flakes is easier than that of H_2SO_4, because the intercalating time of H_2SO_4 into graphite often needs at least 16 h [13] while in the case of $HClO_4$, the intercalating time is less than 0.5 h. (3) The amount of oxidizer, HNO_3, used in the synthesis of $HClO_4$-GIC is by far lower than that used in the synthesis of H_2SO_4-GIC, as can be seen by comparing [14] with [15]. Therefore, it is essential that the mechanical, electrical and thermal performances of FGS derived from $HClO_4$-GIC and its structure characteristics be investigated in order to develop its potentialities as thermal management or electrically heated materials.

Experimental

Raw materials

Natural graphite flakes particles with 99.5 wt% carbon content and average particle size of 2-2.5 mm**,** commercial grade perchloric acid (72 wt%) and nitric acid (65 wt%).

Preparation of $HClO_4$-GIC and FGS

Natural graphite flakes, perchloric acid and nitric acid were used as host material, intercalating agent and oxidizing agent, respectively, to prepare $HClO_4$-GIC. The intercalation reaction temperature is −15 to 100 °C and reaction time is 15–30 min. The mass ratio among natural graphite flakes, nitric acid, and perchloric acid is 1:(0.15–0.20):(3–7). The synthesized $HClO_4$-GIC was subjected to washing, drying to form residue graphite compound. The residue graphite compound then was placed in electrically heated furnace when the temperature was kept at 900 °C and resided 10–30 s to form exfoliated graphite particles. About 3–5 g particles first were evenly spread in a mold with a diameter of 100 mm, and then compressed to form an article with a thickness of 3–5 mm, finally, the article was rolled to form FGS with a thickness of 0.15–2.0 mm.

The measurement of exfoliated volume of exfoliated graphite particles

The exfoliated particles were transferred into a graduated cylinder of 70 mm in diameter, 1000 mL in volume to measure their apparent volume after they were cooled down to room temperature. In order to ensure the measurement accuracy, exfoliated graphite particles of 1000 mL were used. The weight of exfoliated graphite of 1000 mL was obtained by using electronic analytical scale. The apparent volume (cm^3/g) was obtained from 1000 mL divided by the corresponding weight (g) and the average value of measurement results of five times is denoted as EV of exfoliated graphite particles. The EV was used as an index of characterizing the exfoliating ability of $HClO_4$-GIC.

Performance measurement of FGS

The tensile strength was performed on an all-purpose material tester (CMT5000, SNS, Shenzhen, China) controlled by computer according to the ASTM C565 with a cross-head speed of 0.5 mm/min. The five identical samples were used to measure the tensile strength for the same FGS. The arithmetic average values were obtained according to the five test results. The size and shape of the specimens were seen in Ref. [16] The in-plane electrical resistivity was measured by the conventional direct current four-probe method on a milli-ohm meter (Gom-801HDC, Taipei) according to ASTM C611. The size of specimens is 30 × 10 × (0.15–0.20) mm. The test result was obtained by averaging arithmetically over electrical resistivities of three identical samples. The thermal diffusivity (α, mm^2/s) was measured by laser flash method on a laser thermal conduction instrument (Netzch LFA447 Nanoflash^{TM}) according to ASTM C714. The specimen for the in-plane thermal diffusivity measurement is a circular sheet, whose diameter is 20 mm and thickness is 0.1–0.2 mm. For out of plane thermal diffusivity, the specimen is a square sheet whose size is 10 × 10 × (0.15–0.20) mm. Three parallel tests were performed for either the in-plane or the out of plane thermal diffusivity. The thermal conductivity (λ,W/m k) of FGS is calculated by the formula: $\lambda = \alpha \times d \times c$ where d—the density of FGS, g/cm^3; c—the specific heat of FGS (0.85 J/g) [17].

Characterizations

Room temperature X-ray diffraction (XRD) measurements were conducted by using a Brucker-AXSD8 Advance

vertical $\theta/2\theta$ goniometer to obtain X-ray diffraction patterns of samples. The Ni-filtered Kα radiation of copper ($\lambda = 0.154178$ nm) was used. The X-ray diffraction patterns were collected in the $\theta/2\theta$ step scanning mode with a step size of 0.02° (2θ); scanning range, $2\theta = 5°$–$85°$; scanning rate, 4°/min; anodic voltage, 40 kV; and current, 30 mA. Average interlayer spacing, d_{002}, was determined from Bragg equation. The microcrystalline carbon layer stacking height, Lc, was calculated from Scherrer equation. Raman spectroscopy measurements were performed by LABRAM-HR800. The 514 nm line of an Ar-ion laser was used to induce the Raman spectrum. The laser beam was focused on the surface of samples. With the aid of a microscope, which was mounted on top of the sample holder, the illuminated area of the sample could be examined in situ. The illuminated area was set at 20 μm in diameter. The cross-sectional morphology of samples was observed on JEOL JSM-6360 SEM.

Results and discussion

Effects of the shaping force on the density of FGS

Figure 1 shows that the density of the FGS monotonically increases with the shaping force increasing and the lower the EV of exfoliated graphite is, the easier it is pressed into FGS with a higher density (above 1.2 g/cm^3) under the same pressure. The FGS compacted from exfoliated graphite with low EV tends to have low resilience after remove of pressure [18]. This result shows the exfoliated graphite with low EV is easily pressed into the FGS with the higher density due to small resilience.

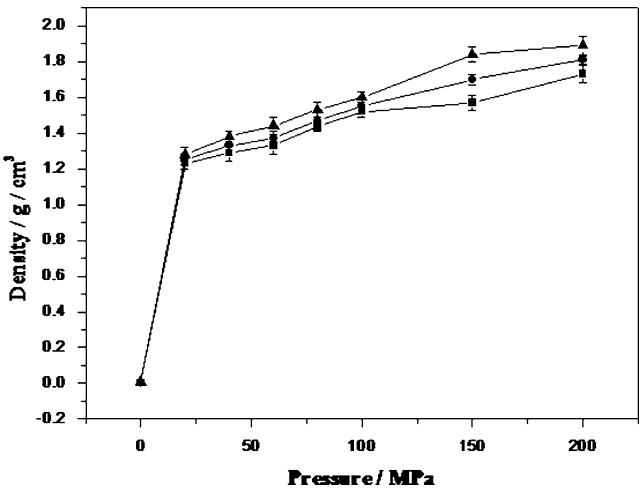

Fig. 1 Density of flexible graphite as a function of pressure (*filled triangle*, *filled circle*, *filled square* represent the FGS compacted from the exfoliated graphite with the EV of 150, 280, 540 mL/g, respectively)

The performances of FGS

Tensile strength

The strength of FGS is dependent not only on the loosing degree of the structure of a heap of exfoliated graphite particles but also on the physicochemical state of the individual particle surface, which is related to both properties of the initial graphite and the conditions used in the chemical and thermal treatment [19]. It can be seen from Fig. 2 that the higher the EV of exfoliated graphite is, the higher the tensile strength of the corresponding FGS is under the same density and the tensile strength of FGS increases with its density increasing. Dowell and Howard [20] and Yang et al. [21] have also concluded that the tensile strength in the plane of foil increases linearly with the density of the foil. Yang et al. concluded that the tensile strength of the foil increases as the diameter of the pristine natural graphite flakes increases. They demonstrated that the increase in the tensile strength with flake size is only realized when the GIC is "fully exfoliated", otherwise the strength may decrease with increasing flake size. We suggest that the underlying relationship of tensile strength to flake size should be that to the EV of exfoliated graphite. The high EV means that it has larger specific surface area and surface energy than that with smaller EV and so it is easily bound together under pressure to form FGS with higher tensile strength.

Electrical and thermal conduction characteristics of FGS

Since FGS is highly anisotropic, its thermal conduction characteristics in both in-plane direction and out of plane direction were investigated. The measurement of electrical

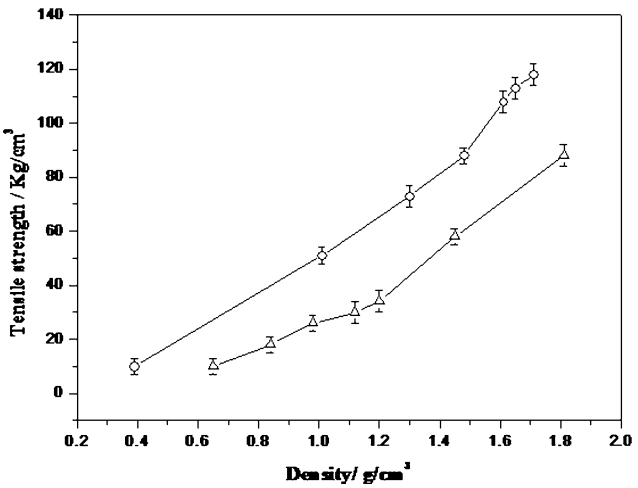

Fig. 2 The tensile strength of FGS with different apparent density (*open circle* and *open triangle* represent the FGS compacted from the exfoliated graphite with 540, 280 mL/g, respectively)

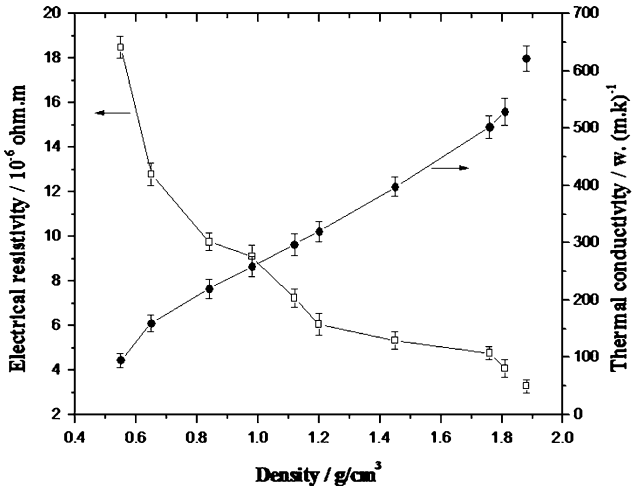

Fig. 3 The relationship of the in-plane electrical resistivity and thermal conductivity of FGS with its density

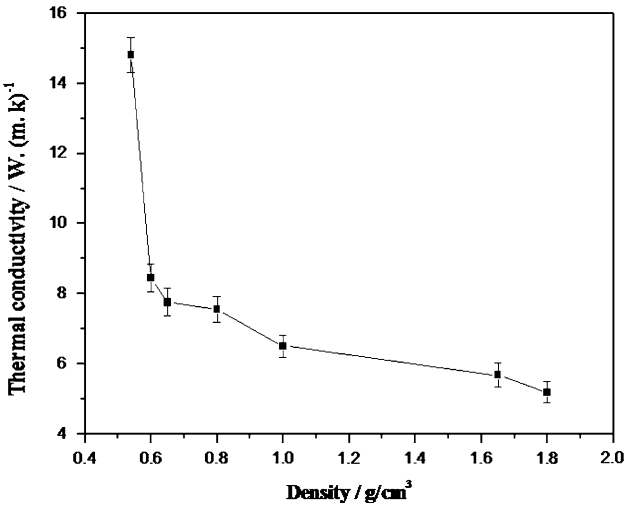

Fig. 4 The relationship of the axial direction thermal conductivity of FGS with its density

resistivity of FGS was finished only in the in-plane direction due to the relevance between electrical conduction and thermal conduction. Figure 3 shows that either electrical or thermal conduction increases with its densities in the in-plane direction. According to the preparing characteristics of exfoliated graphite, it consists of the graphite microcrystals that are exfoliated in the intercalation and subsequently thermal treatment and those that are not exfoliated as can be evidenced by XRD measurement of $HClO_4$-GIC hereinafter. Therefore, there should be four kinds of resistance impeding its in-plane electrical or thermal conduction for FGS: the resistance ($R1$) of microcrystals themselves which keep intact without being intercalated in the intercalation reaction, the resistance ($R2$) of microcrystals themselves which were intercalated by $HClO_4$ and then exfoliated upon heating, the resistance ($R3$) between microcrystals in a single exfoliated graphite particle and the contact resistance ($R4$) of microcrystals between particles. Increasing density contributes to improving the contact area, the orientation of microcrystals, i.e., decreasing $R2$, $R3$, and $R4$ while having no effect on $R1$. Of all the resistances affecting the conductivities of FGS, $R1$ is negligible compared to $R2$, $R3$, and $R4$. Figure 4 shows that the out of plane thermal conductivity (λc) of FGS decreases with its density increasing, as is opposite to the relationship of in-plane thermal conductivity (λa) of FGS with its density. The relation of the axial direction electrical resistivity with the density is similar to the λc—density relation for FGS [22]. This indicates that the thermal conduction anisotropic ratio ($\lambda a/\lambda c$) increases with density increasing. The λc-density behavior is due to the competitive effect of two processes: preferential orientation of elemental graphite planes normal to the compression, which is disadvantageous for the effective thermal conduction along the axis-direction, and the reduction in

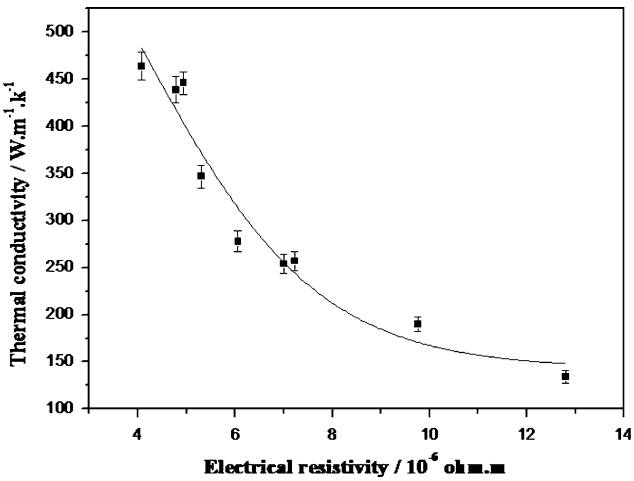

Fig. 5 The relationship between the thermal conductivity and the electrical resistivity for FGS

porosity, which is advantageous for increasing the thermal conductivity. Of the two factors affecting the axis-direction thermal conduction, the preferential orientation maybe is dominant over the reduction in porosity with density increasing. Either the preferential orientation or the reduction in porosity due to density increasing for FGS is favorable to the in-plane thermal conduction. This is the reason why λa increases while λc decreases with density increasing.

Owing to the electrical resistivity (ρ) being an easy measurement parameter compared to the thermal conductivity, therefore, if it were possible to obtain a correlation between them, it would provide a valuable guidance to researchers seeking to optimize thermal conductivity, without having to perform complicated thermal measurements. Figure 5 shows that FGS presents a similar

characteristic in the correlation between ρ and λ with the metal conductors and artificial carbon or graphite articles. The ρ–λ relationship for metal conductors obeys the Weideman-Franz law at room temperature: $\lambda \times \rho =$ constant. The ρ–λ empirical relationship for artificial graphite whose microcrystalline size, La, is more than 20 nm, is $\lambda = 418/(0.293\rho + 0.34)$[23]; for highly oriented mesophase pitch carbon fiber, $\lambda = 4.4 \times 10^5/(100\rho + 258) - 295$ [24]. The empirical expression given by using the sigmoidal regression on the ρ–λ correlation in the in-plane direction for the FGS studied is $\lambda = 102.2 + 1168.4 \exp(-\rho/3.5)$.

Effect of EV of exfoliated graphite on the thermal diffusivity of FGS

Figure 6 indicates that FGS, which was prepared by using exfoliated graphite with low EV, has high thermal diffusivity under the same density (1.65 g/cm^3). The varying trend also holds for the FGS with other densities, although they are not shown here. This is probably due to difference in the numbers of contacts between microcrystals in FGS. The FGS made from exfoliated graphite with larger EV maybe has more numbers of contacts, i.e., the higher contact thermal resistance and inferior microcrystalline graphite layer plane orientation, but these two factors are disadvantageous over thermal conduction.

The XRD structural characterization of FGS

The XRD patterns of FGS, along with natural graphite flakes, $HClO_4$-GIC, exfoliated graphite for comparative purpose are presented in Fig. 7. The $HClO_4$-GIC sample for XRD analysis has a EV of 540 cm^3/g at 900 °C, which is the maximum EV value obtained in $HClO_4$-HNO_3-natural graphite flakes system. The exfoliated graphite was obtained by thermally exfoliating the $HClO_4$-GIC at 900 °C. The density of FGS is 1.7 g/cm^3. It can be seen from Fig. 7 that (002) peaks for natural graphite flakes (a), FGS (b), GIC (c), and exfoliated graphite (d) located at 26.553°, 26.552°, 26.113°, and 26.308°, respectively. According to the Bragg equation, the d-spacing (d_{002}) values for natural graphite flakes, GIC, exfoliated graphite and FGS are 3.357, 3.412, 3.388, and 3.357 Å, respectively. The average stacking height (Lc) of graphite microcrystallites was obtained from Scherrer equation. The instrumental broadening had been deducted in calculating the Lc. The corrected width (w) is determined from the formula $w = \left(w_1^2 - w_0^2\right)^{1/2}$, where w_1 is the full width at half maximum height of 002 diffraction peak from sample and w_0 is the instrumental width and amounts to 0.15° expressed in terms of 2θ, which is determined from highly pure crystalline silicon. The Lc values for natural graphite flakes, GIC, exfoliated graphite and FGS are 331, 137, 236, and 236 Å, respectively. The fact that FGS has almost the same Lc and d_{002} as exfoliated graphite indicates that the shaping pressure has almost no effect on the microcrystal structure in the compressing exfoliated graphite particles. The XRD pattern (Fig. 7c) of $HClO_4$-GIC suggests inhomogeneous structure, intercalated and not-intercalated. If so, the exfoliated graphite is also inhomogeneous, some flakes were exfoliated but others are not. The diffraction intensity of (002) peaks for natural graphite flakes, FGS, $HClO_4$-GIC, and exfoliated graphite decreases sequentially. This indicates that the shaping pressure tends to increase the orientation of microcrystals. As far as orientation is concerned, the pristine natural graphite is the best while exfoliated graphite is the worst and FGS is between them according to their respective XRD intensities.

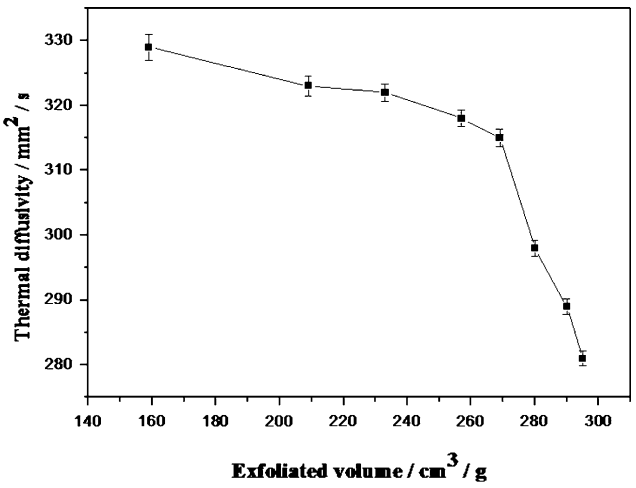

Fig. 6 The relationship between the thermal diffusivity of FGS and the EV of exfoliated graphite, a precursor for making FGS under the same density (1.65 g/cm^3)

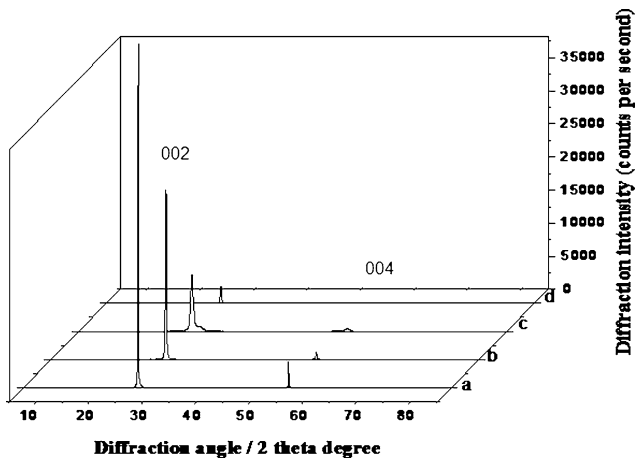

Fig. 7 XRD patterns of *a* natural graphite flakes, *b* FGS, *c* $HClO_4$-GIC, *d* exfoliated graphite

The cross-section morphology of FGS

SEM was used to characterize the cross-section morphology of FGS. It can be seen that the graphite flake layer orientation in FGS prepared from exfoliated graphite with low EV (Fig. 8a) is superior to that in FGS prepared from exfoliated graphite with high EV (Fig. 8b) under the same density (1.7 g/cm^3). It is explained structurally that why using exfoliated graphite with the low EV tends to enhance the thermal conductivity of resultant FGS.

The Raman spectra of natural graphite flakes, exfoliated graphite, and FGS

The normal Raman spectrum for a typical carbonaceous material consists of two peaks, one around 1360 cm^{-1} called D peak (disordered) and another around 1580 cm^{-1} called G peak (graphite), the former being structure-sensitive and absent in the spectra of graphite single crystals [25–28]. The 1360 cm^{-1} band has been assigned to a vibrational mode originating from the distorted hexagonal lattice of graphite near the crystal boundary, and can be, therefore, observed for ordinary carbon materials containing various defective structures in the graphite layers planes, i.e., a defective-induced Raman vibrational mode [29]. For graphite, the characteristic G peak is associated with the E_{2g} vibrational mode—vibrations of the carbon atoms within the hexagonal sp^2 network of the graphite layer. The mode at 1580 cm^{-1}, often referred as the G mode, is assigned to "in-plane" displacement of the carbon strongly coupled in the hexagonal sheets. Its shifts and linewidth variations are indicative of the defects in the lattice [30]. The Raman spectra of FGS, along with exfoliated graphite and natural graphite flakes for comparative purpose are shown in Fig. 9. The existence of D peak indicates that natural graphite flakes, exfoliated graphite, and FGS are typical polycrystalline graphite materials because graphite single crystal has only one G peak in Raman spectrum [31]. Of natural graphite flakes, exfoliated graphite and FGS, natural graphite flakes possess the strongest Raman G band while FGS has the weakest G band, which is probably due to the difference of orientation of graphite microcrystalline layers in local region. According to the attribution of D band, exfoliated graphite should have the strongest D band compared to natural graphite flakes and FGS, but really not, as is opposite to the results obtained in exfoliating carbon fiber [32]. Yang et al. [33] examined the Raman spectrum characteristics of exfoliated graphite samples obtained at different exfoliation temperatures. They obtained a result that the ratio of intensity of D to G band (I_D/I_G) decreases with exfoliating temperature increasing. They suggested that high exfoliating temperature help improve the structure of graphite crystals. This implies that the exfoliated graphite with large EV has low I_D/I_G value, as is accordance with our Raman testing result on exfoliated graphite. According to Fig. 9,

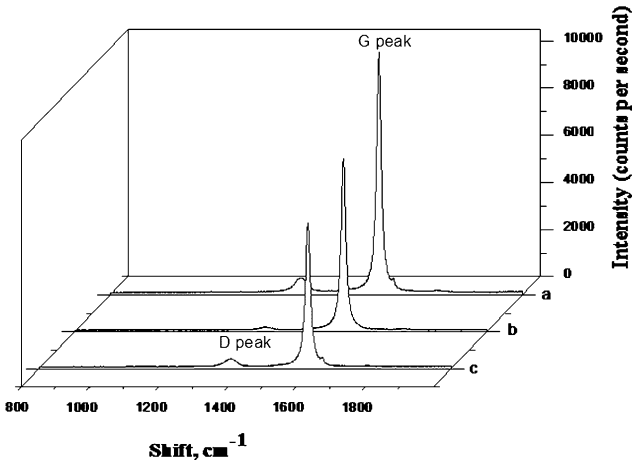

Fig. 9 Raman spectra of FGS, exfoliated graphite and natural graphite flakes

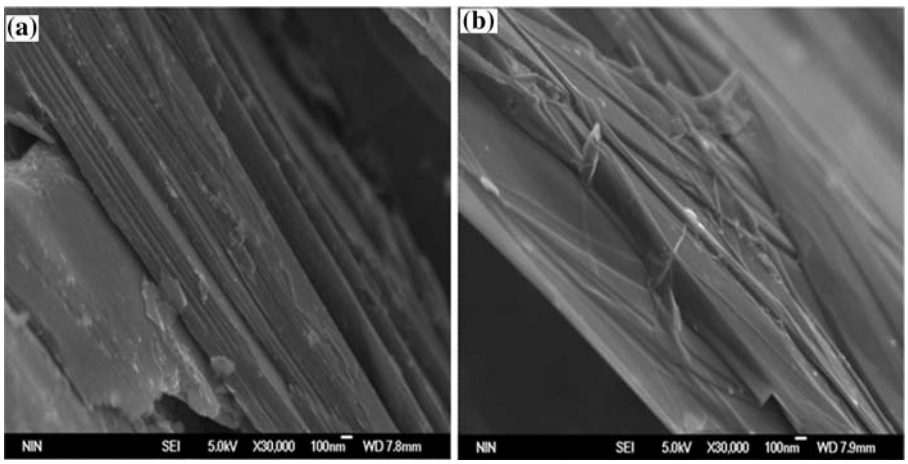

Fig. 8 SEM micrographs of the transverse morphology of FGS prepared using exfoliated graphite with different EV (**a** 64 cm^3/g; **b** 384 cm^3/g)

FGS has almost as the same I_D/I_G (ca. 0.060) as natural graphite flakes while the I_D/I_G value of exfoliated graphite is ca. 0.014. We suggest that interior stress should be responsible for this phenomenon because exfoliated graphite maybe has more low interior stress than FGS or natural graphite flakes due to exfoliation. According to the G peak intensity, as far as the orientation of microcrystals is concerned, FGS is between EG and NGF.

Conclusions

FGS based on $HClO_4$-GIC has good in-plane mechanical, electrical, and thermal performances. The maximum in-plane tensile strength, thermal conductivity, and minimum electrical resistivity are 12 MPa, 620 W/m k, and 3.3 μΩ m, respectively. The in-plane thermal conductivity increases with density increasing while the out of plane thermal conductivity decreases with density increasing. The tensile strength, electrical resistivity, and thermal conductivity of FGS in the in-plane direction are closely related to both its density and the apparent bulk density of exfoliated graphite from which FGS is made. The empirical expression on the correlation between the thermal conductivity (λ, W/m k) and the electrical resistivity (ρ, μΩ m) in the in-plane direction for the FGS studied is $\lambda = 102.2 + 1168.4 \exp(-\rho/3.5)$. The exfoliated graphite with low EV tends to produce FGS with high thermal conductivity. The XRD results show that the average interlayer spacing, d_{002} of FGS is 3.357 Å which is the same as that of natural graphite flakes, but its average stacking height, Lc, is lower than that of natural graphite flakes. The low EV of exfoliated graphite does help improve the thermal conduction of FGS according to SEM morphology observations. The Raman spectra indicate that FGS has both G and D peaks, the intensity ratio of D to G peak being ca. 0.06 which is almost the same as that of natural graphite flakes, but higher than that of exfoliated graphite. The internal stress and the orientation of graphite microcrystalline layers are probably main two factors influencing the G or D bands of Raman spectra for natural graphite flakes, exfoliated graphite, and FGS.

References

1. Inagaki M, Kang FY (2006) Carbon materials science and engineering—from fundamentals to applications. Tsing University Press, Peking
2. Redchitz AV, Ionov SG, Avdeev VV (2006) J Phys Chem Solids 67:1202
3. Celzard A, Mareche E, Furdin G (2005) Prog Mater Sci 50:93
4. Chung DDL (2000) J Mater Eng Perform 9:161
5. Hoi YM, Chung DDL (2002) Carbon 40:1134
6. Inagaki M, Suwa T (2001) Carbon 39:915
7. Toyoda M, Aizawa J, Inagaki M (1998) Desalination 115:199
8. Toyoda M, Inagaki M (1999) Tanso 187:96
9. Toyoda M, Inagaki M (2000) Carbon 38:199
10. Toyoda M, Moriya K, Aizawa J, Konno H, Inagaki M (2000) Desalination 128:205
11. Inagaki M, Konno H, Toyoda M, Moriya K, Kihara T (2000) Desalination 128:213
12. Toyoda M, Moriya K, Aizawa J, Konno H, Inagaki M (2000) Desalination 128:219
13. Chen GH, Wu DJ, Weng WG, Wu CL (2005) Carbon 41:579
14. Nakajima T, Matsuo Y (1994) Carbon 32:469
15. Wei XH, Liu L, Zhang JX (2007) New Carbon Mater 22:342
16. Gu JL, Yang L, Gao Y, Liu H, Kang FY, Shen WC (2002) Carbon 40:2169
17. Bonnissel M, Luo L, Tondeur D (2001) Carbon 39:2151
18. Gu JL, Cao WQ, Shen WC, Liu YJ (1996) New Carbon Mater 11:49
19. Pyatkovskii ML, Mikhaillova LL, Sementsov YI (2001) Powder Metall Met Ceram 40:464
20. Renolds RA, Greinke RA (2001) Carbon 39:473
21. Yang L, Gu JL, Cao WQ, Zhang TY (1998) Carbon 36:875
22. Chung DDL (1987) J Mater Sci 22:4190. doi:10.1007/BF01132008
23. Kelly BT (1969) In: Walker PL (ed) The chemistry and physics of carbon. Dekker, New York
24. Lavin JG, Boyington DR, Lahijani J (1993) Carbon 31:1001
25. Sato Y, Kamo M, Setaka N (1978) Carbon 16:279
26. Compagnini G, Puglsi O, Foti G (1997) Carbon 35:1793
27. Kawashima Y, Katagiri G (1999) Phys Rev B 59:62
28. Pocsik I, Hundhausen M, Koos M, Ley L (1998) J Non-Cryst Solids 230:1083
29. Nakamizo M, Honder H, Inagaki M (1978) Carbon 16:281
30. Tse HK, Wen SK (2002) Polym Compos 21:745
31. Tuinstra F, Koenig JL (1970) J Chem Phys 53(3):1126
32. Toyoda M, Kaburagi Y, Yoshida A (2004) Carbon 42:2567
33. Yang JG, Wu CP (2006) Chin J Fight Scatt 17:341